Spectral Signatures of Polar Stratospheric Clouds and Sulfate Aerosol

S. T. MASSIE, P. L. BAILEY, AND J. C. GILLE

National Center for Atmospheric Research,† Boulder, Colorado

E. C. LEE*

Princeton University, Princeton, New Jersey

J. L. MERGENTHALER, A. E. ROCHE, AND J. B. KUMER

Lockheed Palo Alto Research Laboratory, Palo Alto, California

E. F. FISHBEIN AND J. W. WATERS

Jet Propulsion Laboratory, California Institute of Technology, Pasadena, California

W. A. LAHOZ

University of Reading, Reading, United Kingdom

(Manuscript received 21 March 1994, in final form 13 July 1994)

ABSTRACT

Multiwavelength observations of Antarctic and midlatitude aerosol by the Cryogenic Limb Array Etalon Spectrometer (CLAES) experiment on the *Upper Atmosphere Research Satellite* are used to demonstrate a technique that identifies the location of polar stratospheric clouds. The technique discussed uses the normalized area of the triangle formed by the aerosol extinctions at 925, 1257, and 1605 cm^{-1} (10.8, 8.0, and 6.2 μm) to derive a spectral aerosol measure M of the aerosol spectrum. Mie calculations for spherical particles and T-matrix calculations for spheroidal particles are used to generate theoretical spectral extinction curves for sulfate and polar stratospheric cloud particles. The values of the spectral aerosol measure M for the sulfate and polar stratospheric cloud particles are shown to be different. Aerosol extinction data, corresponding to temperatures between 180 and 220 K at a pressure of 46 hPa (near 21-km altitude) for 18 August 1992, are used to demonstrate the technique. Thermodynamic calculations, based upon frost-point calculations and laboratory phase-equilibrium studies of nitric acid trihydrate, are used to predict the location of nitric acid trihydrate cloud particles.

1. Introduction

Polar stratospheric clouds alter stratospheric chemistry by providing surface area upon which heterogeneous chemistry shifts the partitioning between active chlorine and chlorine reservoir species (Solomon et al. 1986). With the transition from polar night to day, photolytic release of chlorine radicals leads to substantial chemical ozone loss [see chapter 4 of WMO (1991) for a review of chemical/dynamical processes associated with the Antarctic ozone hole]. There are two main types of polar stratospheric clouds (PSCs). PSC I clouds form at temperatures near and below 195 K and are expected to be composed of nitric acid trihydrate (Toon et al. 1986; Crutzen and Arnold 1986; Turco et al. 1989). At colder temperatures, below the frost point of water, PSC II clouds form and are composed of water ice.

The focus of this paper is to demonstrate a way to distinguish between the sulfate aerosol and PSC particles by using multiwavelength observations of aerosol extinction in the infrared. Observations from the Cryogenic Limb Array Etalon Spectrometer (CLAES) on the *Upper Atmosphere Research Satellite (UARS)* are used to demonstrate the technique. Mie calculations are performed to calculate theoretical aerosol extinction spectra for sulfate aerosol, nitric acid trihydrate (NAT) particles, and water ice particles. It is shown that the spectral characteristics expected for the three types of particles are different. Since the NAT and ice particles

* Current affiliation: Stanford University, Palo Alto, California.

† The National Center for Atmospheric Research is sponsored by the National Science Foundation.

Corresponding author address: Dr. S. T. Massie, National Center for Atmospheric Research, P.O. Box 3000, Boulder, CO 80307.

may be nonspherical, T-matrix calculations (Barber and Hill 1990) are performed to explore the effect of particle shape upon the extinction spectra. Using CLAES data, aerosol extinction values at 925, 1257, and 1605 cm^{-1} are used to form a spectral aerosol measure M derived from the normalized area of the triangle formed by these three extinction values. The theoretical calculations are used to predict the range of M values for the sulfate and PSC particles (i.e., sulfate particles have M between -1 and -2, and PSC particles have M between 0 and 1.5). The CLAES data are then used to calculate observed M values, which are compared to the theoretical predictions.

Previous laboratory studies (Hanson and Mauersberger 1988) have specified the range of temperature, H_2O partial pressure, and HNO_3 partial pressure for which NAT particles are expected to exist. Using the Hanson and Mauersberger data, it is shown below that many of the observed data points are at ambient temperatures below the temperature threshold for NAT (as specified by observed temperature, H_2O, and HNO_3 values) and also have M values as suggested by the theoretical extinction model for PSCs.

There are several studies that have examined the spectral signatures of sulfate aerosol and that of PSC particles. Halperin and Murcray (1987) compared theoretical sulfate aerosol and observed spectral radiances for the range 8.7–13.4 μm (746–1149 cm^{-1}). Observed spectral radiances were obtained by a balloonborne grating spectrometer. The theoretical radiances incorporated Mie calculations based upon measured particle size distributions before and after the April 1982 eruption of El Chichón. General agreement between the theoretical spectral radiance values and observation (for September 1982, over Palestine, Texas) was found when the aerosol size distribution corresponded to stratospheric measurements in September 1982, over Utah. In contrast, the theoretical curve using the background aerosol level (before the El Chichón eruption) had low radiance values when compared to the observation. In another study, Pollack et al. (1991) compared theoretical and observed transmission data for the range 4.5–13.5 μm (740–2222 cm^{-1}). The observations were obtained by a filter wheel spectrometer on the NASA Convair 990, which flew at approximately 11-km altitude in December 1982 and April/May 1983. The data were highly influenced by the presence of the El Chichón dust cloud. Spectral features due to CH_4, N_2O, O_3, H_2O, and sulfuric acid aerosol are present in the data. Theoretical curves, which display the contribution of each species to the total transmission spectrum, indicate that sulfuric acid aerosol makes an important contribution to the total transmission spectrum.

Cirrus cloud spectral signatures may serve as a useful analog to type II PSC spectra, since both cloud types are composed of water ice. Spectral signatures of cirrus and altocumulus clouds have been observed using the High (spectral) Resolution Interferometer Sounder (HIS) (Ackerman et al. 1990). During the First ISCCP Region Experiment (FIRE), simultaneous lidar and high–spectral resolution infrared observations of cirrus clouds were taken from the NASA ER2 in 1986. The HIS observations demonstrate that cirrus clouds cannot be considered to be gray (i.e., have a flat spectral signature) in the region 8–12 μm. Ackerman et al. proposed a three-channel detection technique using spectral measurements near 8, 11, and 12 μm as a way to separate clear regions, cirrus clouds, and liquid water clouds. Retrieval of cloud properties using a continuous range of HIS data between 800 and 1200 cm^{-1} is discussed by Smith et al. (1993).

The Stratospheric Aerosol Measurement (SAM) II satellite experiment has made measurements of polar stratospheric clouds since October 1978. SAM II measures profiles of aerosol extinction at a wavelength of 1.0 μm. Since SAM II is a solar occultation experiment, observations in winter view up to the edge of the polar night. However, the latitude ranges covered, 64° to 82°S for the Antarctic winter and 64° to 82°N for the Arctic winter, have provided a very extensive climatology for PSCs. PSC extinction coefficients at 1.0 μm are as much as two orders of magnitude greater than the background stratospheric aerosol extinction values (McCormick et al. 1982). The occurrence of PSCs is shown to be dependent upon temperature. Clouds are observed 90% of the time when the temperature is less than 185 K, and 45% of the time when the temperature is less than 193 K (McCormick et al. 1982). The extinction in the polar region has been studied during both background level and volcanically disturbed periods (McCormick and Trepte 1986). Histograms of PSC occurrence for the years 1979–87 for the southern polar regions have been determined (McCormick et al. 1989). The SAM II data have also provided information on the geographical distribution of Antarctic stratospheric clouds (Watterson and Tuck 1989).

Observations of the spectral dependence of PSC particle extinction obtained during the 1987 Airborne Antarctic Ozone Expedition were reported by Kinne et al. (1989). The data were obtained aboard a DC-8 flying in the 10–11-km altitude range, by the Jet Propulsion Laboratory (JPL) Mark IV interferometer, at solar zenith angles greater than 80°. The interferometer operated in the range 1.8–15 μm. Estimates of average particle radius, mass loading, and type (i.e., ice, nitric acid trihydrate) were made by comparing the observed wavelength dependence of the extinction with several theoretical models. Simultaneous measurements of nitric acid vapor by the same instrument displayed lower HNO_3 concentrations in the presence of PSCs, supporting the view that the type I PSCs contain nitric acid.

Additional information on PSCs have been derived from analysis of lidar observations. The NASA Langley airborne differential absorption lidar (DIAL) flew during the 1988–89 Airborne Arctic Stratospheric Ex-

pedition and observed PSCs in the altitude range 14–17 km (Browell et al. 1990). Two types of PSC I particles, at temperatures less than 195 K, were observed. Type Ia particles had low scattering ratios (1.2–1.5) and high aerosol depolarization (30%–50%), while type Ib particles had high scattering ratios (3–8) and low aerosol depolarizations (0.2%–2.5%). Water ice PSCs were observed to have high scattering ratios (>10) and high aerosol depolarizations (>10%) at temperatures less than 190 K. Analysis of the Browell depolarization data by Toon et al. (1990) attributed lidar observational characteristics to PSC I particles, which are small (type Ib particles, radius 0.5 μm, spherical) and large (type Ia particles, 1.0 μm, not quite spherical), and to nonspherical PSC type II ice particles.

While this paper only uses aerosol extinction from the CLAES experiment, other *UARS* instruments also measure sulfate aerosol and PSC extinction. *UARS* studies of the Mount Pinatubo sulfate cloud started soon after the 12 September 1991 launch of *UARS*. The MLS (Microwave Limb Sounder) experiment observed the conversion of SO_2 into HSO_3 starting 100 days after the 15 June 1991 eruption of Mount Pinatubo (Read et al. 1993). ISAMS (Improved Stratospheric and Mesospheric Sounder) data was used by Grainger et al. (1993) to study the infrared absorption spectrum of the Mount Pinatubo cloud and by Lambert et al. (1993) to illustrate graphically the evolution of the Mount Pinatubo cloud. Mergenthaler et al. (1993) used CLAES data to report on 1992 Southern Hemisphere sulfate aerosol and Antarctic PSC distributions. HALOE (Halogen Occultation Experiment) extinction data are compared to correlative measurements by Hervig et al. (1993).

2. CLAES experiment

CLAES is one of ten experiments on *UARS* (Reber et al. 1993). The CLAES instrument is composed of a telescope, transfer optics, a set of blocker filters, Fabry–Perot etalons, and an array of 23 solid state detectors at the focal plane, coupled to a passive solid Ne/solid CO_2 cooler (Roche et al. 1993). During an observation sequence, one etalon and one blocker filter are used in conjunction to observe at several wavenumbers within the bandpass of the blocker filter. Angular rotation of the etalon allows CLAES to scan through a range of wavenumbers. There are nine blocker filter regions, centered at 780, 790, 840, 879, 925, 1257, 1605, 1897, and 2843 cm^{-1} (12.82, 12.65, 11.90, 11.36, 10.83, 7.95, 6.23, 5.27, and 3.52 μm). The blocker filters vary in width between 3 and 10 cm^{-1}. Spectral resolution of the four Fabry–Perot etalons varies between 0.19 and 0.65 cm^{-1}.

Species that contribute to the emission spectra viewed by CLAES are CO_2, O_3, H_2O, HNO_3, NO_2, N_2O, CH_4, CFC-12, CFC-11, N_2O_5, $ClONO_2$, NO, HCl, and several continua. The sources of continua are sulfate aerosol, the pressure-induced absorption of oxygen (in the 1605 cm^{-1} region), clouds in the upper troposphere, and polar stratospheric clouds. Production processing of CLAES observations solves for the pressure–temperature profiles, the mixing ratios of many of the species listed above, plus the continua (NASA 1994).

Version 6 data are used in this study. The production processing reports an extinction coefficient (km^{-1}) for many of the CLAES blocker regions. For the blocker centered at 1605 cm^{-1}, the extinction data are those due to all continua within the blocker region. A correction due to the presence of the pressure-induced absorption of molecular oxygen is applied to the data in order to extract the aerosol component. For the blocker centered at 1257 cm^{-1}, the production processing attempts to remove the contribution of N_2O_5 to the total radiance, using a climatological N_2O_5 value for the daytime. During nighttime viewing the production software solves simultaneously for the aerosol and N_2O_5. The extinction in the 1257 cm^{-1} blocker region is therefore due just to aerosol. The daytime aerosol extinction alone is used in this study since validation studies (NASA 1994) indicate that the nighttime 1257 cm^{-1} aerosol extinction is underestimated by 33%.

Due to the precession of the *UARS* orbit, *UARS* undergoes a 180° yaw around every 36 days. The 57° inclination of the satellite restricts observations from CLAES to latitudes between 80°N and 20°S (for the northward-looking phase) and 20°N and 80°S (for the southern-looking phase). Data from the southward-looking phase centered on 18 August 1992 are examined in this paper. As noted in Fig. 3-1 of WMO (1991), the sighting frequency of PSCs in the Antarctic, as observed by the SAM II instrument, peaked in August for the years between 1979 and 1989.

UARS data is classified as level 1, 2, and 3, depending upon the form of the data. Level 1 and level 2 data are calibrated instrument data and geophysical (retrieved) profile data, respectively. Level 3 data is a mapped product. In this paper, we have used the level 3 AT mapped data, which is the production software version of level 2 data mapped to common time boundaries. The level 3 AT data was then transformed by us to a latitude–longitude grid, using a hybrid approach of Cressman (1959) and Kalman (1960) filter techniques, which map and average over space and time. Daytime-mapped fields were produced for all observables in the study (i.e., temperature, aerosol extinction, and H_2O and HNO_3 mixing ratio fields). Longitude–pressure cross sections of aerosol extinction, presented below, are based upon our mapped version of the *UARS* level 3 AT data.

The following sections focus upon data at 46 hPa, a pressure level at which the aerosol extinction error bars are generally smaller than those at other pressure levels

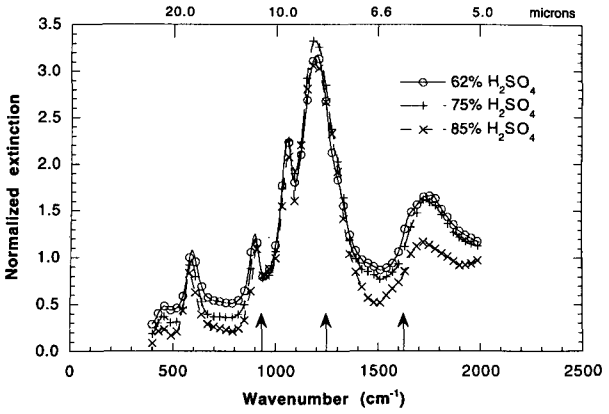

FIG. 1. Theoretical aerosol extinction for sulfate aerosol at 62%, 75%, and 85% H_2SO_4 (by weight). The curves are normalized to one at 925 cm^{-1}. Arrows point to CLAES observations at 925, 1257, and 1605 cm^{-1} (10.83, 7.95, and 6.23 μm).

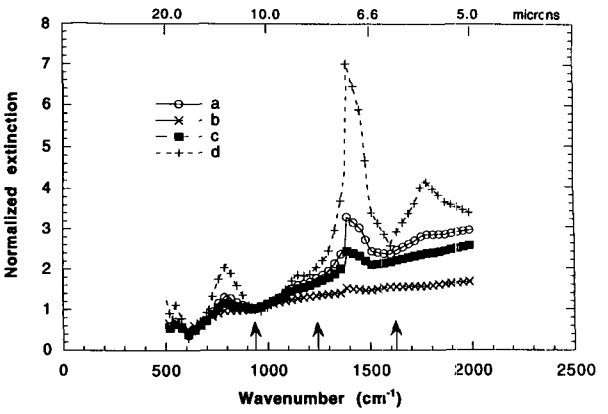

FIG. 2a. Theoretical PSC extinction for NAT particles, normalized to one at 925 cm^{-1}. Arrows point to CLAES observation wavenumbers at 925, 1257, and 1605 cm^{-1} (10.83, 7.95, and 6.23 μm). See Tables 1 and 2 for the conditions that apply for curves a, b, c, and d.

(NASA 1994). The 46 hPa is also a pressure level at which PSCs are frequently observed. Quality indicators (error bars) are included in the *UARS* database for each level 2 data point (for each temperature, mixing ratio, aerosol extinction value, etc.). Performing an average of these quality indicators over the latitude range of 18° to 20°N, within which sulfate aerosol is present, error bars are on the order of 12%, 13%, and 8% at 925, 1257, and 1605 cm^{-1}. An average of the quality indicators for the latitude range from 68° to 72°S in the polar vortex yields error bars on the order of 35%, 31%, and 16%. These values are applicable to the PSC extinction at temperatures below 195 K and at extinction values greater than 3.0×10^{-4}, 6.0×10^{-4}, and 6.0×10^{-4} at 925, 1257, and 1605 cm^{-1}. Both sets of error bars are used in section 7 to calculate the uncertainties involved in the determination of the aerosol measure M. Since mapped fields of aerosol extinction are used in our analysis, these error bars likely overestimate the random component of the uncertainty of the mapped extinction data.

3. Extinction model

Mie and T-matrix calculations are used to model theoretically the wavenumber dependence of the sulfate and PSC extinction for the 400 to 2000 cm^{-1} range. Observed size distributions of sulfate and PSC particles, plus refractive indexes of the sulfate and NAT materials, are used as inputs to the theoretical calculations. These theoretical calculations are used to support the technique discussed below, which identifies PSC and sulfate particles from distinct spectral signatures.

Figure 1 presents theoretical curves of sulfate aerosol extinction at 62%, 75%, and 85% H_2SO_4 (by weight), based upon the size distribution of Deshler et al. (1993), which corresponds to 20 km over Laramie, Wyoming, on 8 August 1992. The particles are derived from the Mount Pinatubo eruption of June 1991; that is, the sulfate aerosol has a concentration appreciably above that of a volcanically quiet period. Indexes of refraction of H_2SO_4 used in the Mie calculations are those of Palmer and Williams (1975). Each of the curves in Fig. 1 is normalized to unity at 925 cm^{-1}. The arrows in Fig. 1 mark the observation wavenumbers for the CLAES data at 925, 1257, and 1605 cm^{-1}, which are used in this study. Using the three data pairs of aerosol extinction and wavenumber at the three designated observation wavenumbers, one forms a triangle with a substantial height. As discussed below, this triangle forms the basic geometrical shape from which a normalized area is formed and from which the spectral aerosol measure M is calculated.

Model PSC extinction spectra, based upon Mie calculations, are displayed in Figs. 2a and 2b. The theoretical extinction spectra in these figures are based upon

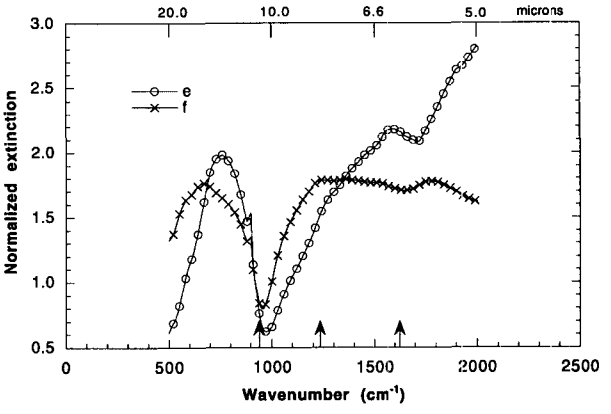

FIG. 2b. Theoretical PSC extinction for ice particles, normalized to one at 925 cm^{-1}. Arrows point to CLAES observation wavenumbers at 925, 1257, and 1605 cm^{-1} (10.83, 7.95, and 6.23 μm). See Tables 1 and 2 for the conditions that apply for curves e and f.

the particle size distributions of Hofmann and Deshler (1991) and Deshler et al. (1991). These observations were obtained in September 1989 and 26 August–7 October 1990, respectively, at altitudes between 15 and 21 km, over McMurdo Station, Antarctica. Extinction curves for both nitric acid trihydrate (curves a, b, c, and d) and water ice particles (curves e, f) are presented in Figs. 2a and 2b. Table 1 presents the date, altitude, and particle composition, and Table 2 presents the lognormal particle size parameters of the bimodal particle size distributions. Particles corresponding to the size distributions used to calculate curves e and f in Fig. 2b are expected to be water ice particles, since if the particles were NAT, then the inferred source HNO_3 vapor mixing ratio associated with the particles would be unrealistically large. The spectra in Fig. 2 are calculated within the limitations of the Mie theory, which applies to spherical particles. (Calculations for nonspherical PSC particles are discussed in subsequent paragraphs.) Refractive indexes of water ice (Warren 1984) were used to calculate the extinction curves of the PSC II particles. For the nitric acid trihydrate particles, the imaginary indexes of refraction are based upon the absorbance data displayed in panel 3b of Tolbert and Middlebrook (1990). Application of the relationship (Feynman 1964)

$$\tau = 2\omega n_{im} z/c \qquad (1)$$

is used to estimate the wavenumber dependence of the imaginary index of refraction n_{im}, where

τ absorbance (optical depth) of the thin film (dimensionless)
ω circular frequency of the infrared beam (rad s^{-1})
z thickness of the laboratory thin film (cm)
c speed of light (cm s^{-1}).

For the real index of refraction, a value of 1.4 is assumed for NAT between 500 and 2000 cm^{-1}.

The CLAES observation wavenumbers at 925, 1257, and 1605 cm^{-1} are also displayed in Fig. 2 by the arrows. The triangles formed by the three data pairs of aerosol extinction and wavenumber for curves a–f have a flattened appearance (the triangle has a small height).

The difference in appearance of the sulfate aerosol extinction and PSC extinction curves can be understood from examination of Mie calculations. The aerosol extinction is given by the equation

$$\text{aer}(i) = 1.0 \times 10^{-3} \int Q_{\text{ext}} \pi r^2 (dn/dr) dr, \qquad (2)$$

where

$Q_{\text{ext}}(m, r, \lambda)$ Mie extinction coefficient (dimensionless)
m complex index of refraction (dimensionless)
λ wavelength (μm)
r particle radius (μm)
dn/dr particle size distribution (particles/cm^3 μm).

Graphs of the integrand of Eq. (2) versus particle radius at 925, 1257, and 1605 cm^{-1} show that the sulfate aerosol and PSC particles have maximal contributions to the integral at different radii. For example, using the sulfate and PSC particle size distributions discussed above, the sulfate and PSC integrand curves have maximal contributions near 0.5 and 5 μm, respectively. In Mie theory (van de Hulst 1975), the quantity $2\pi r/\lambda$ is referred to as the particle size parameter x. A typical Q versus x curve increases as x increases from $x = 0$ to larger x, to largest Q for x in the range of 2 to 5, followed by oscillatory values of Q at larger x. The Q values finally settle down to a value of Q equal to 2 at the largest x values. The sulfate aerosol particles have maximal contributions to Eq. (2) for x near one-half, whereas the PSC particles have maximal contributions near x of four. The Q versus x curves have larger differences in Q value at 925, 1257, and 1605 cm^{-1} for the sulfate aerosol for x near one-half, and in a relative sense, smaller differences in Q for x near four for the PSC particles. Thus, the extinction at 925, 1257, and 1605 cm^{-1} differs more for the sulfate aerosol than for the PSC particles. This accounts for the difference in shape of the triangles formed by the sulfate and PSC extinction at these three wavenumbers.

In quantitative terms, the normalized triangle for an aerosol observation is based upon the following transformations:

TABLE 1. PSC size distributions used to prepare Figs. 2a and 2b.

Curve	Altitude (km)	Pressure (hPa)	Temperature (K)	Composition
a	21	30	186	NAT
b	19	47	189	NAT
c	20	39	188	NAT
d	16	75	193	NAT
e	17	63	187	ICE
f	15	96	194	ICE

TABLE 2. Bimodal size distributions used to prepare Figs. 2a and 2b.

Curve	N_1 (cm^{-3})	r_1 (μm)	σ_1	N_2 (cm^{-3})	r_2 (μm)	σ_2
a	13.0	0.033	2.67	0.0048	1.82	1.54
b	11.0	0.057	1.64	0.0072	1.39	2.03
c	11.0	0.050	2.23	0.0003	2.70	1.24
d	8.0	0.091	1.70	0.0071	2.00	1.53
e	10.1	0.084	1.66	0.0577	3.01	1.32
f	10.0	0.094	1.82	0.0042	7.65	2.40

N_i: total particle number density for distribution $i = 1,2$ r_i: mean radius, and σ_i: distribution width.

$$x_i = (\text{wave}(i) - \text{wave}(1))/d\text{wave} \quad (3)$$

$$y_i = (\text{aer}(i) - \text{aer}(2))/\text{aer}(2), \quad (4)$$

where

$$i = 1, 2, 3 \quad \text{for } 925, 1257, 1605 \text{ cm}^{-1};$$

and

aer(i) the aerosol extinction (km^{-1}) at the wavenumber for observation i
wave(i) the wavenumber for observation i
$d$wave wave(3) − wave(1).

With the three pairs (x_i, y_i), one can form the normalized area A of the triangle by

$$A = \frac{1}{2}\begin{vmatrix} 1 & 1 & 1 \\ x_1 & x_2 & x_3 \\ y_1 & y_2 & y_3 \end{vmatrix}, \quad (5)$$

where | | denotes the absolute value of the determinant of the matrix. It is then useful to transform the area A by way of the equation

$$M = 1.5 - (10.0A). \quad (6)$$

This transformation and the calculations presented in Figs. 1 and 2 yield M values of −1.4, −1.7, and −1.8 for the 62%, 75%, and 85% H_2SO_4 concentrations of the sulfate aerosol, and M values between +0.7 and +1.2 for the PSC size distributions. If the H_2SO_4 concentration were to become as low as 40% or 50%, then the M values would be −0.4 and −1.0, respectively. Note that since A is greater than or equal to zero, M is always less than 1.5.

Uncertainties in the indexes of refraction of sulfuric acid solutions and of the solid phase lead to uncertainties in the theoretical calculations of the aerosol spectral measure M values. Measurements of the room temperature indexes of refraction of sulfuric acid solutions are discussed by Palmer and Williams (1975) and by Remsberg et al. (1974). The Palmer and Williams measurements are tabulated for H_2SO_4 concentrations at 95.6%, 84.5%, 75%, 50%, 38%, and 25% for the 400 to 27 800 cm^{-1} range. The Remsberg measurements are cited at 90% and 75% H_2SO_4 concentrations for the 747–1571 cm^{-1} range. Palmer and Williams cite a fractional uncertainty of 1% for the real indexes and an uncertainty of 3% for the imaginary indexes. The Palmer and Williams real indexes agree with the Remsberg measurements (for 75% H_2SO_4) to 2%. The Remsberg imaginary indexes, however, are 5% to 10% larger than the Palmer and Williams indexes between 1000 and 1571 cm^{-1} and are 25% larger between 747 and 1000 cm^{-1}. Using the larger values for the imaginary indexes, the spectral measure M at 75% H_2SO_4 changes from −1.70 to −1.37.

An important uncertainty is due to the lack of published indexes of refraction at cold stratospheric temperature. The Lorentz–Lorenz equation can be used to extrapolate the indexes of refraction from room temperature to colder temperatures. Use of the Lorentz–Lorenz equation, however, has known limitations. In the study of Pinkley and Williams (1976), the Lorentz–Lorenz equation appeared to be valid away from absorption bands but problematic near strong absorption bands. Recent studies of the $H_2SO_4/H_2O/HNO_3$ system have observed changes in thin-film absorbance spectral features for the 180 to 230 K temperature range (Middlebrook et al. 1993; Molina et al. 1993). In the experiments of Middlebrook, sulfuric acid tetrahydrate (SAT) formed at temperatures between 180 and 200 K (with the temperature threshold dependent upon several experimental conditions). Once formed, SAT melted at temperatures between 216 and 219 K. Middlebrook presents absorbance spectra at room temperature and for the range 180 to 230 K, which display changes in structure (e.g., changes in spectral shape and in the locations of the peak features) as temperatures and H_2SO_4 concentrations decrease. Improvement in the quantitative calculation of aerosol spectra awaits quantification of the indexes of refraction for the sulfuric acid solution and solid phase at cold temperatures.

The transformation for M in Eq. (6) is of graphical convenience, since the sulfate aerosol then has M values in the negative range, and the PSC aerosol has M values in the positive range. The reason for using a normalized extinction is that stratospheric aerosol can be patchy. An altitude profile of extinction is also nonuniform. The normalized quantity A and spectral measure M can be used to mark the location of sulfate aerosol and PSC particles by a single number, which is independent of the magnitude of the aerosol extinction but dependent upon the characteristic spectral signatures of the two types of particles.

The papers of Hofmann and Deshler (1991) and Deshler et al. (1991) list two dozen size distributions for NAT particles and two distributions for ice particles. The aerosol measure values for this set of size distributions has a range of M between 0 and 1.4. The calculations for the ice particles do not sample well the full set of possible ice crystal spectra, since only two distributions are included in the Mie calculations. The predicted aerosol measure M values for the PSC and sulfate size distributions are presented in Fig. 3. The sulfate aerosol and the PSC data points fall into distinct groups.

4. Calculations for nonspherical particles

The discussion above assumes that the PSC particles can be represented by spheres. To assess the influence of particle shape upon the theoretical extinction curves, calculations were performed upon a range of particle shape for both the PSC I and II particles. The calculations used the T-matrix program of Barber and Hill (1990). Although the T-matrix approach is applicable to particles of arbitrary shape, the Barber and Hill code

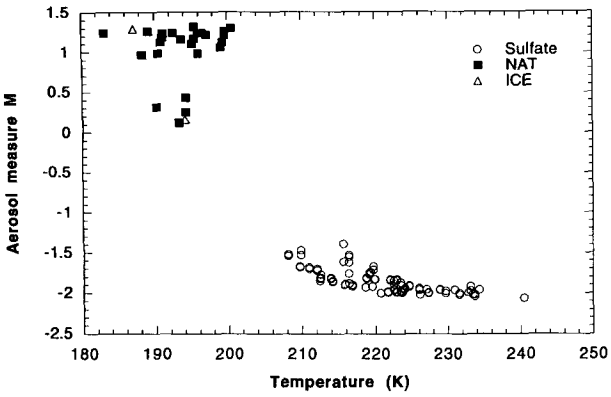

FIG. 3. Graphical representation of the theoretical calculations of the aerosol measure M for measured PSC and sulfate aerosol size distributions.

is applied to axisymmetric spheroidal particles. Particle shape is specified by the eccentricity ratio E of major to minor axis. Effective $Q_{\text{extinction}}$ values for Eq. (2) were obtained by calculating the ratio $(\sigma/\pi\alpha^2)$, where α is the radius of a sphere equal in volume to the nonspherical particle, and σ is the spatially averaged extinction cross section for a particle size distribution with particles randomly oriented.

As discussed by Toon et al. (1990), PSC I particles may deviate from spherical shape, since laboratory NAT crystals grown from liquid were observed to have an eccentricity E value near 1.2 (Taesler 1975). Toon et al. (1990) also interpret lidar observations of PSCs, who support the idea that PSC I particles deviate from spherical shape as the particles become larger in size. Photomicrographs of PSC I particles, collected on Formvar coated substrates, show imprints of spheres or droplets (Pueschel et al. 1992), so the spherical assumption is likely to hold at least for a portion of the PSC I population.

Using identical imaginary indexes of refraction and one PSC I size distribution T-matrix calculations were carried out for values of E between 1.0 and 1.4. The M values, based upon the T-matrix calculations for particles with major/minor axis ratios between 1.0 and 1.4, differed by the order of one percent. The absolute magnitude of the extinction, however, decreased by 15% as E varied from 1.0 to 1.4. These results suggest that although M values for spherical particles differ from more realistic calculations by a small amount, the Mie calculation will overestimate the absolute extinction value.

In contrast to the NAT particles, the PSC II ice particles are known to be nonspherical. Goodman et al. (1989) obtained ice crystal replicas during ER-2 flights at altitudes between 12 and 18 km, during which the temperature varied between 190 and 201 K. Solid and hollow columns were frequently observed, though some ice cubes (at the higher temperatures) and a few trigonal plates also were observed. Major axis values between 11 and 49 μm were observed, with variations in length/diameter ratios between 1.2 and 2.7. A representative particle was solid, with a major axis of 12 μm and a length/diameter ratio near 2.

Calculations for ice particles for a range of E from 1.0 to 3.5 were performed using the Warren (1984) ice indexes and the particle size distributions e and f of Fig. 2b. Values of the aerosol spectral measure M decreased from near 1 to near 0 as E varied between 1.0 and 2.5. The Mie calculation ($E = 1$) overestimated the particle extinction by a factor of 4, in comparison to the T-matrix $E = 2.5$ calculation. These results reveal the influence of the shape factor E upon M. The spectral measure M becomes negative for ice distribution f when E becomes larger than 2. These results imply that PSC II ice particles will likely have spectral measures M near zero.

5. Sulfate aerosol

To illustrate the spectral signature of sulfate aerosol, *UARS* data for 18 August 1992 are examined at temperature latitudes. Figure 4 presents a longitude–pressure graph of temperature for 20°N latitude, based upon the temperature fields reported by the *UARS* Microwave Limb Sounder (MLS). The Version 3 MLS temperature fields are represented as a piecewise linear function with breakpoints at alternate (even numbered) *UARS* pressure surfaces (e.g., 46, 22, 10 hPa). At pressure greater than 22 hPa, the profiles are linearly interpolated from National Meteorological Center (NMC) daily analyses (or climatology when necessary) onto the even-numbered surfaces. In the following discus-

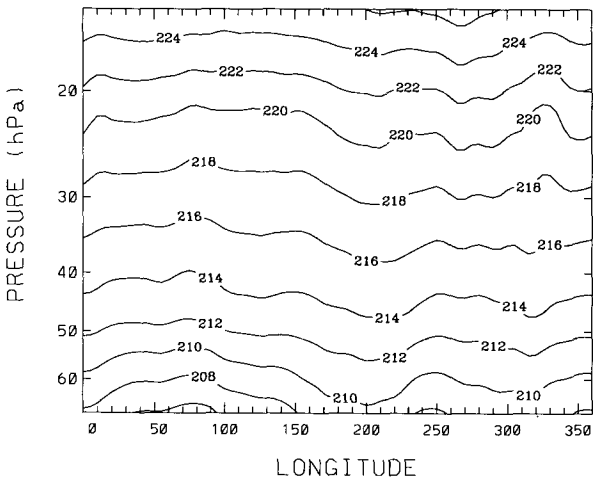

FIG. 4. MLS temperatures at 20°N latitude on 18 August 1992 for pressures between 10 and 70 hPa. These temperatures are above the range of temperature at which PSC particles form. Daytime temperatures are displayed. The temperatures at pressures greater than 22 hPa are from the National Meteorological Center.

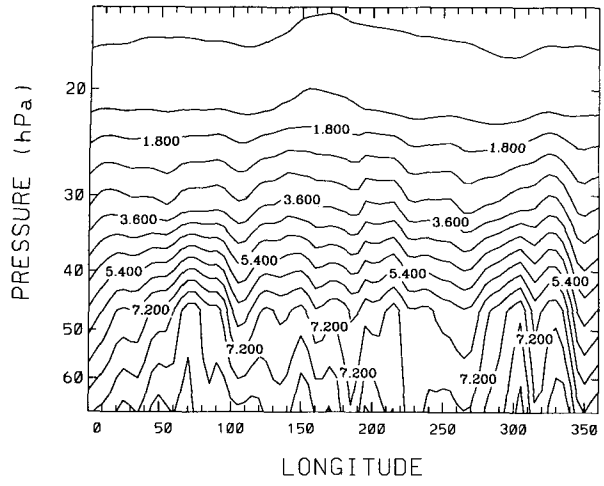

FIG. 5. CLAES daytime aerosol extinction, in units of 1.0 $\times 10^{-4}$ km^{-1}, at 925 cm^{-1} at 20°N latitude on 18 August 1992.

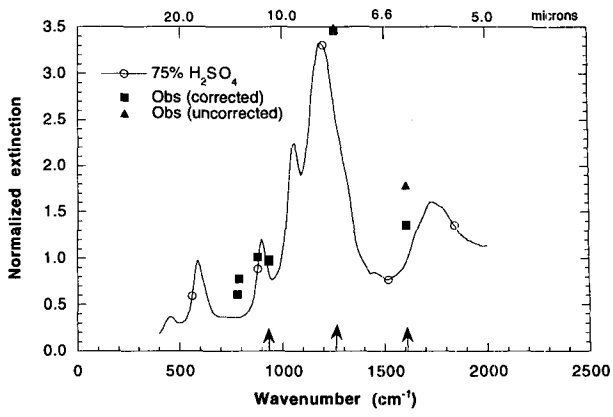

FIG. 6. Comparison of theoretical and CLAES observations of sulfate aerosol. Both sets of data have been normalized to 1 at 925 cm^{-1}. The CLAES observations correspond to 20°N, 10°E and 46 hPa. Data points at 1257 and 1605 cm^{-1} show extinction uncorrected and corrected for the presence of N_2O_5 and the pressure-induced absorption of oxygen, respectively. The theoretical curve corresponds to 75% H_2SO_4.

sion, for the 46-hPa surface, the temperature error budget is that associated with the NMC datasets.

The temperatures in Fig. 4 are above 208 K, that is, at temperatures above the thresholds of PSC I and PSC II formation. Figure 5 presents CLAES aerosol extinction at 925 cm^{-1} for the same conditions as in Fig. 4. The field of aerosol extinction shows little longitudinal structure between 20 and 50 hPa. For this pressure range, the aerosol extinction falls off in magnitude as pressure decreases. Error bars associated with the level 3 AT data and validation studies indicate that the CLAES aerosol fields are physically meaningful for the range 20 to 50 hPa and become less certain at higher and lower pressure levels (NASA 1994).

Figure 6 displays CLAES data at 20°N latitude, 10° longitude, 46 hPa (near 21 km altitude) on 18 August 1992 for 780, 790, 879, 925, 1257, and 1605 cm^{-1}. Figure 6 also displays a theoretical sulfate aerosol curve. The theoretical curve was calculated using a H_2SO_4 concentration based upon application of the equilibrium H_2SO_4 table of Steele and Hamill (1981), in which the observed temperature profile was used to calculate the H_2SO_4 percent concentration (by weight). Though there are quantitative differences between observation and theory in Fig. 6, the observations do conform to the general structure of the theoretical curve, with a high value of extinction at 1257 cm^{-1} and lower values of extinction at the other observation wavenumbers.

As mentioned above, the processed CLAES extinction data represent all continua at 1605 cm^{-1}, while a climatological N_2O_5 contribution to the 1257 cm^{-1} observation has been subtracted from the total retrieved continua. The upper data point in Fig. 6 was calculated by adding an approximate per kilometer contribution due to N_2O_5 at 1257 cm^{-1} [calculated by using a mid-latitude mixing ratio value of N_2O_5 from the Atmospheric Trace Molecule Spectroscopy (ATMOS) experiment in conjunction with laboratory absorption cross-sectional data for N_2O_5]. The correction due to N_2O_5 is seen to be small in this example (the square and triangle overlap in Fig. 6). The correction for the pressure-induced absorption (PIA) of oxygen at 1605 cm^{-1} is, however, appreciable. The extinction due to the aerosol and the PIA is given by the topmost point in Fig. 6. The lower point at 1605 cm^{-1} is obtained by subtracting out the PIA from the topmost point.

The PIA absorption coefficients of Orlando et al. (1991) are used in the subtraction process. The Orlando coefficients measured between 225 and 356 K extrapolate well to a temperature of 195 K (based upon

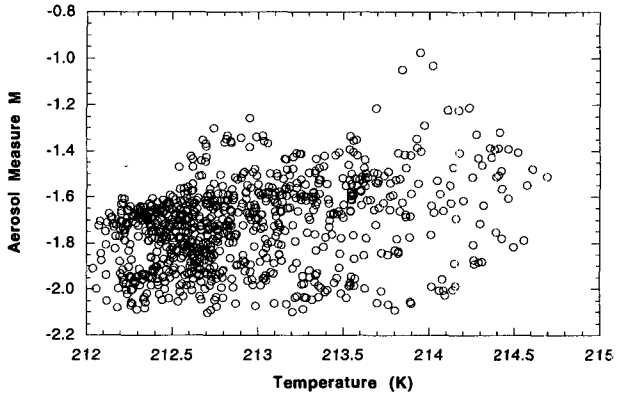

FIG. 7. Aerosol spectral measure M values for latitudes between 20°S and 20°N at all longitudes and at 46 hPa on 18 August 1992. Values of M between −1.5 and −2.0 indicate the presence of sulfate aerosol.

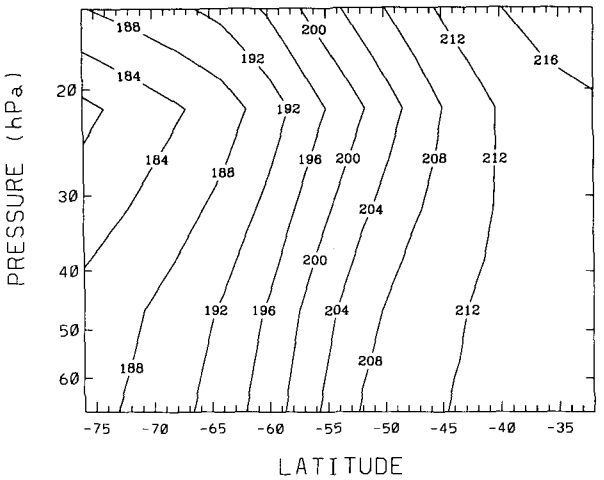

FIG. 8. MLS temperature field at 290°E longitude on 18 August 1992 for pressures between 10 and 70 hPa. Daytime temperatures are displayed. The temperatures for pressures greater than 22 hPa are from the National Meteorological Center.

comparison of the extrapolated value to another study at 195 K). Using the CLAES extinction at 925, 1257, and 1605 cm^{-1} in Fig. 6, a spectral measure M equal to -1.79 is obtained, implying the presence of sulfate aerosol.

Figure 7 presents a scatter diagram of temperature and aerosol measure M for data on 18 August 1992, for the latitude range $-28°$S to $+20°$N at 46 hPa. The range of temperature is between 212 and 215 K. PSC particles are not expected to be present at these latitudes and temperatures. The aerosol spectral measure M values are expected to be those of sulfate particles, which is supported by Fig. 7; that is, PSC M values greater than zero are not present.

The 46-hPa surface was chosen to illustrate the sulfate aerosol spectral measure M values in Fig. 7 since the discussion below focuses on the PSC spectral signature at the 46-hPa pressure level. The MLS instrument on *UARS* detects large ClO mixing ratios in the polar latitudes for altitudes near 20 km at 46 hPa (Waters et al. 1993). Scatter diagrams in the style of Fig. 7 for pressure levels at 68 and 31 hPa, however, also display aerosol spectral measure values between -1.0 and -2.0, and average M values near -1.5, which is characteristic of sulfate aerosol. This is expected, since sulfate aerosol exists throughout the altitude range 15 to 25 km. For the 21-hPa surface, the scatter diagram of M with temperature reveals a large amount of scatter. The aerosol extinction at 1605 cm^{-1} at 21 hPa is roughly a factor of 10 lower than the extinction at 68 and 46 hPa. These low extinction values have large error bars and, therefore, large uncertainty in the derived M values.

6. PSC aerosol

At temperatures near and below 195 K, one expects to observe the development of PSC I particles and, at temperatures below the frost point of water, the development of type II particles. Figure 8 displays MLS temperatures for 18 August 1992 at longitude 290°E, given as a function of pressure and latitude. At latitudes poleward of 60°S, temperatures are below 200 K. At 72°S latitude, MLS temperatures are presented as a function of pressure and longitude in Fig. 9. Temperatures range between 205 and 180 K, and one expects that both PSC I and PSC II particles could reside in these cold temperature regimes. As discussed above, the temperatures in the MLS datasets for pressures greater than 22 hPa are NMC temperatures.

Figures 10a–c show CLAES extinction at 925, 1257, and 1605 cm^{-1} at 72°S latitude as a function of pressure and longitude for 18 August 1992. All three panels show a concentration of extinction between 270° and 320° longitude, and between 35 and 60 hPa. The most intense extinction is seen near 300° longitude. There is a dip in extinction amount for longitudes between 100° and 150°. As discussed below, these extinction patterns are related to the zonal temperature structure of the Antarctic vortex.

Figure 11 presents CLAES extinction at 780, 790, 879, 925, 1257, and 1605 cm^{-1} for 72°S latitude, 290° longitude, and 46 hPa. The 1605 cm^{-1} data point was corrected for the pressure-induced absorption of molecular oxygen. The theoretical curve corresponds to curve c in Fig. 2a and to a size distribution measured at 39 hPa (near 19 km). Forming the normalized area A and spectral measure M the data points in Fig. 11 have a spectral measure M of $+0.2$, which implies the presence of PSC particles.

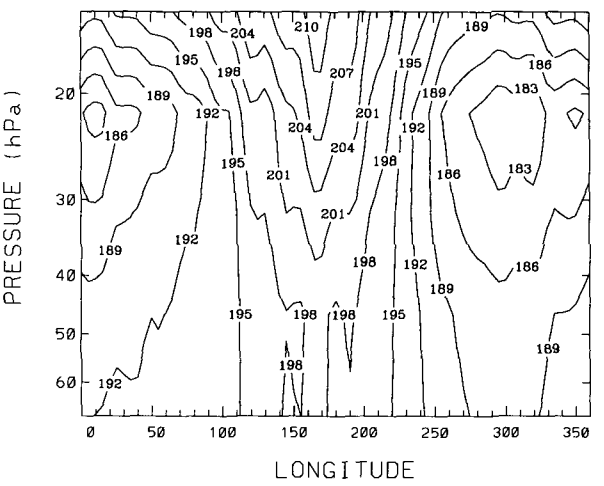

FIG. 9. MLS temperature field at 72°S latitude on 18 August 1992 for pressures between 10 and 70 hPa. Daytime temperatures are displayed. The temperatures for pressures greater than 22 hPa are from the National Meteorological Center.

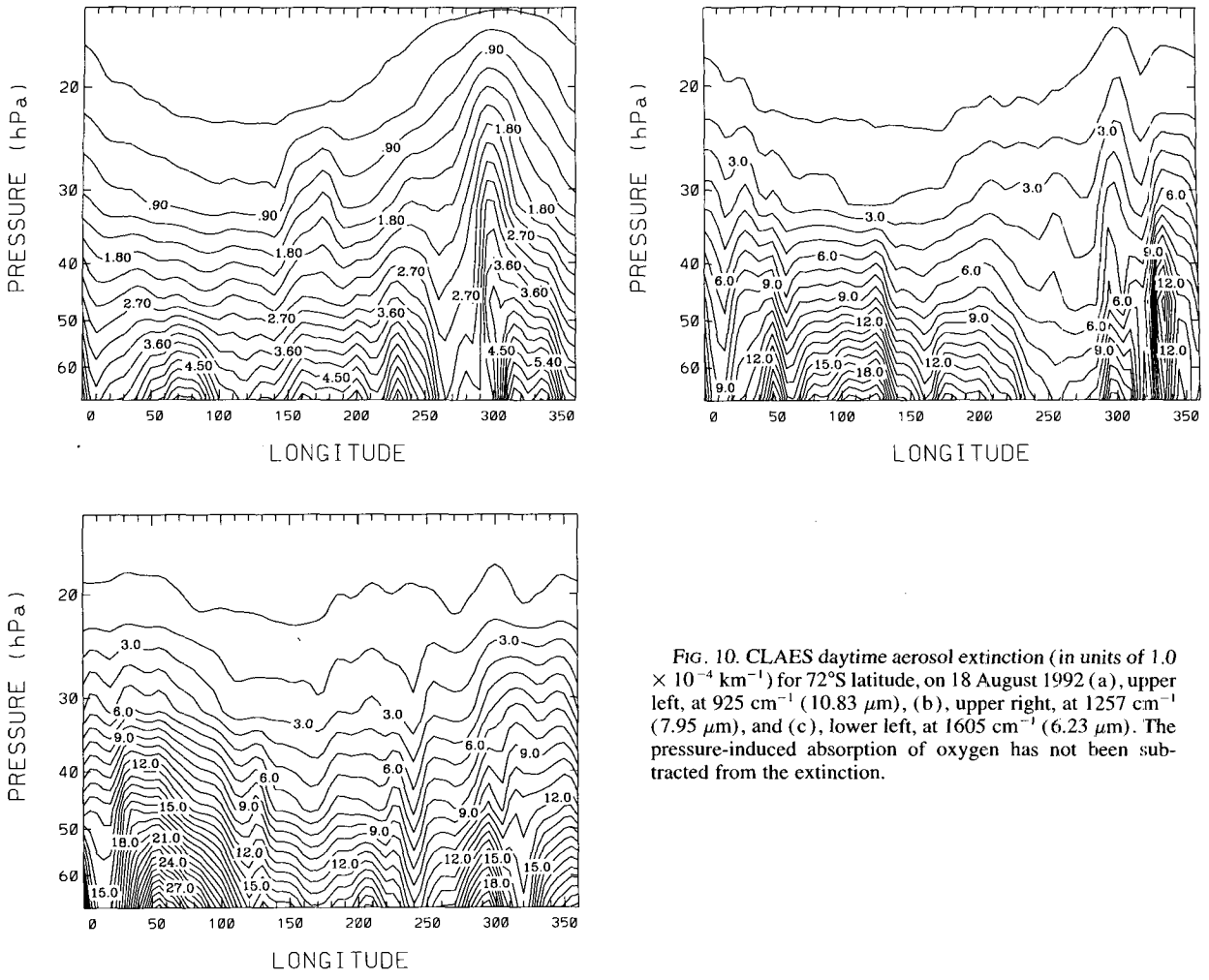

FIG. 10. CLAES daytime aerosol extinction (in units of 1.0 $\times 10^{-4}$ km^{-1}) for 72°S latitude, on 18 August 1992 (a), upper left, at 925 cm^{-1} (10.83 μm), (b), upper right, at 1257 cm^{-1} (7.95 μm), and (c), lower left, at 1605 cm^{-1} (6.23 μm). The pressure-induced absorption of oxygen has not been subtracted from the extinction.

It is expected that the enhanced extinction observed in Figs. 10a–c occur near 300° longitude. Longitudes over the Palmer Peninsula and over the Wedell Sea are known to exhibit frequently the presence of PSCs. Watterson and Tuck (1989) determined the longitudinal distribution of PSCs for the June–October period of 1987, as observed by the SAM II experiment. Observing at 1 μm, SAM II measured background sulfate aerosol and extinction enhancements due to PSC particles. The peak of the PSC extinction was observed near 19 km, though this peak lowered in height from 20 to 15 km throughout the four-month observational period. Histograms of PSC occurrence favored PSCs for longitudes between 240° and 360°. Half of the PSC formation was located over the Palmer Peninsula or southern Wedell Sea. The Palmer Peninsula roughly spans the longitude range 290°–300°, and the Wedell Sea spans the longitude range 300°–350°. While low temperature was a prerequisite for PSC formation, PSCs formed rarely over East Antarctica, even though temperatures were cold enough for PSC formation. The SAM II data also showed that PSCs rarely formed over the center of the vortex. Watterson and Tuck (1989) emphasized the role of dehydration processes in the vortex center due to particle sedimentation and the requirement of the presence of condensable material for the PSC formation process.

Figure 12a presents SAM II PSC incidence rates as determined by Watterson and Tuck for moderate aerosol extinction and for locations in which the latitude of the observations passed over the Palmer Peninsula. Figure 12b presents a bar graph of the number of individual cases for which CLAES aerosol extinction data had values of M greater than 0.0, that is, suggestive of the signature of PSCs. The data in Fig. 12b are for the latitude range 76° to 64°S (latitudes within the polar vortex) and are for the days 18–21 August 1992. Figures 12a and 12b are similar in having maximal incidence rates in the longitude ranges 210°–360° and 0°–60°, and low incidence rates between 60° and 210° longitude. There are some differences between the relative ratio of the maxima at 300° and 20° longitude. In Fig. 12c, average temperatures for the longitude bands are displayed for the 18–21 August time period, with the

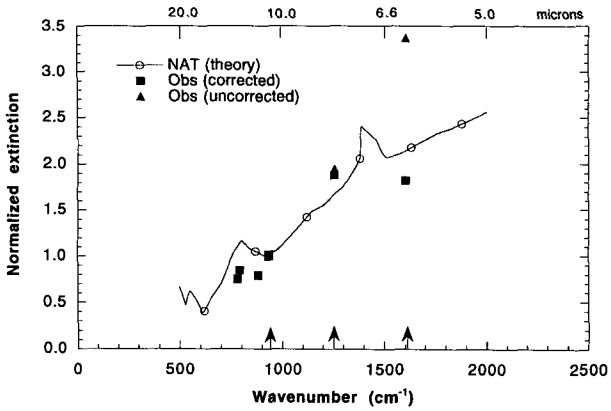

FIG. 11. Comparison of theoretical and CLAES observations of PSC extinction. Both sets of data have been normalized to 1 at 925 cm^{-1}. Data points at 1257 and 1605 cm^{-1} show extinction uncorrected and corrected for the presence of N_2O_5 and the pressure-induced absorption of oxygen, respectively. The theoretical curve corresponds to curve c of Fig. 2a.

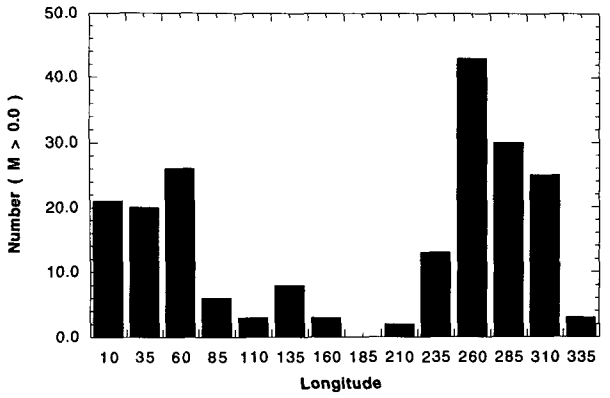

FIG. 12b. Number of cases for which the aerosol spectral measure M was greater than 0 for CLAES data on 18–21 August for latitudes between 76° and 64°S at 46 hPa.

averaging taking place for latitudes between 76° and 64°S. The PSC incidence rate is observed to be high when the average temperature is low. At higher temperatures, for longitudes between 60° and 235°, low incidence rates of PSCs are observed. This is reasonable, since higher temperatures will evaporate the PSCs.

The temperature dependence of the CLAES extinction at 925, 1257, and 1605 cm^{-1} is displayed in Figs. 13a–c. The aerosol extinction is for the latitude range 76° to 56°S at 46 hPa on 18 August 1992, and the aerosol extinction at 1605 cm^{-1} was corrected for the presence of pressure-induced continuum of O_2. There are several common characteristics to the three sets. All three sets show enhanced aerosol extinction for temperatures between 210 and 220 K. These data points are due to the presence of Mount Pinatubo aerosol and

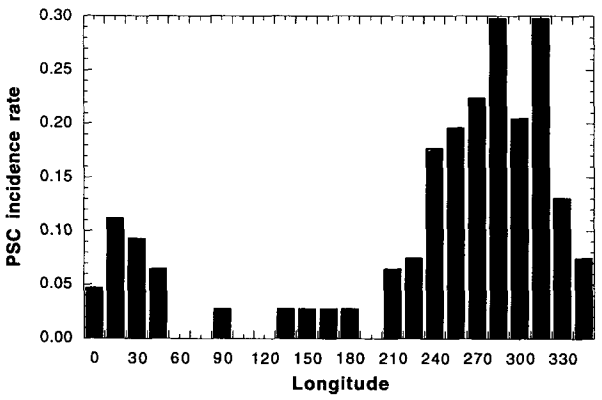

FIG. 12a. PSC incidence rate as determined by Watterson and Tuck (1989) from SAM II data, for moderate aerosol amount and for latitudes that pass over the Palmer Peninsula.

are revealed by comparing scatter diagrams (similar to Figs. 13a–c) for the latitude ranges 76° to 56°S and 52° to 32°S. The 76° to 56° data do not show the enhanced extinction, while the 52° to 32°S data do for the higher temperatures, which are associated with the enhanced aerosol loading at latitudes closest to the equator. All three sets show enhanced extinction at temperatures below 192 K. These data points are associated with the cold stratospheric temperatures within the polar vortex and likely are due to PSC particles. Graphs of temperature, water vapor, and nitric acid versus latitude all show decreases in values for latitudes poleward of 63°S and mark the polar vortex. Graphs of aerosol extinction versus latitude show aerosol increases poleward of 63°S.

As temperatures increase above 195 K, the three scatter diagrams in Figs. 13a–c have one dissimilar feature, in that the 1257 cm^{-1} extinction becomes more enhanced at higher temperatures, as compared to the extinction at 925 and 1605 cm^{-1}. This is characteristic of the sulfate aerosol (see Fig. 1, which shows that the 1257 cm^{-1} extinction is larger than the extinction at 925 and 1605 cm^{-1}). Finally, the scatter diagrams show some outliers. In Fig. 13c, for example, there are a few data points near a temperature of 214 K that are appreciably above the others.

7. Temperature dependence of the aerosol measure *M*

One way to illustrate the spectral characteristics of the sulfate and PSC particles is to plot values of the aerosol measure M as a function of temperature for a wide range of latitude and longitude. Figure 14 displays M values versus temperature for 18 August 1992 for the latitude band between 76° and 36°S, at the 46-hPa pressure level. Seven hundred eighteen individual observations went into the graph. For temperatures greater than 205 K, the M values are generally less than

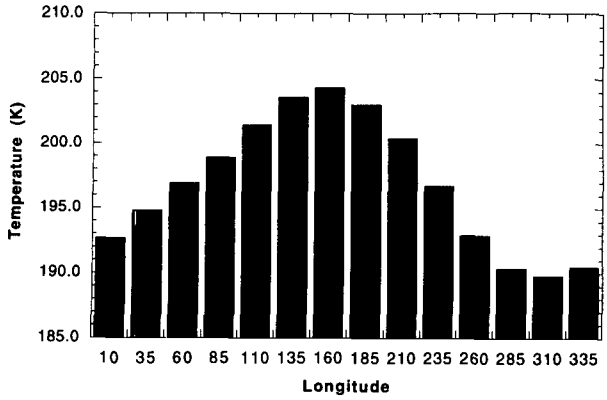

FIG. 12c. Averages of MLS temperatures along longitude lines for 18–21 August, for latitudes between 76° and 64°S, at 46 hPa. The MLS temperatures at 46 hPa are National Meteorological Center temperatures.

−1, which indicates the presence of the sulfate aerosol. At temperatures less than 190 K, there are data points with M greater than 0. Based upon the theoretical calculations discussed above, these data points are likely due to the presence of PSC particles.

It is expected that there is a range of temperature for which sulfate aerosol and PSC particles will coexist and yield an aerosol extinction spectral curve influenced by both particle types. To assess this possibility, values of M were calculated for mixtures of air having both sulfate aerosol and PSCs. The PSC extinction was based upon a Deshler et al. (1991) PSC I size distribution at 21-km altitude, observed on 26 August 1990 over McMurdo. The sulfate extinction was based upon the Deshler et al. (1993) particle size distribution on 2 October 1991 over Laramie, Wyoming, at 21-km altitude. The Wyoming data were divided by 10, which then yielded an extinction spectrum with a value close to that of the PSC extinction spectrum at 1605 cm^{-1}. Table 3 presents M values based upon these two distributions, as the partitioning between PSC and sulfate amounts varied between 0 and 1. (To be more precise, the "amount" refers to aerosol optical depth at 1605 cm^{-1}. A mixture of 0.5 sulfate aerosol and 0.5 PSC refers to equal tangent ray path optical depth contributions by both particle types.) The pure sulfate case yielded $M = -1.75$, while the pure PSC case gave $M = +1.1$. A 50%–50% mix of PSC and sulfate aerosol produced $M = -0.33$. Some of the data points for temperatures near 195 K with M in the range 0 to −1 could be due to a mixture of PSC and sulfate aerosol particles.

Data for the 46-hPa pressure surface are displayed in Fig. 14 since this pressure level, near 20-km altitude, was frequently observed by the SAM II instrument to show PSC particles (Watterson and Tuck 1989). The SAM II PSC peak near 19 km, however, lowered in height from 19 to 15 km throughout the SAM II observational period. Scatter diagrams in the style of Fig. 14 for the pressure levels at 68 and 31 hPa are similar to Fig. 14. For temperatures near 215 K, which are above the expected temperature for NAT and water ice formation, the aerosol spectral measure values are between 0 and −2, characteristic of sulfate. The aerosol spectral measure M values range between −2 and +1.5, similar to those in Fig. 14. The scatter diagram at 21 hPa is very noisy, which is likely due to the fact that

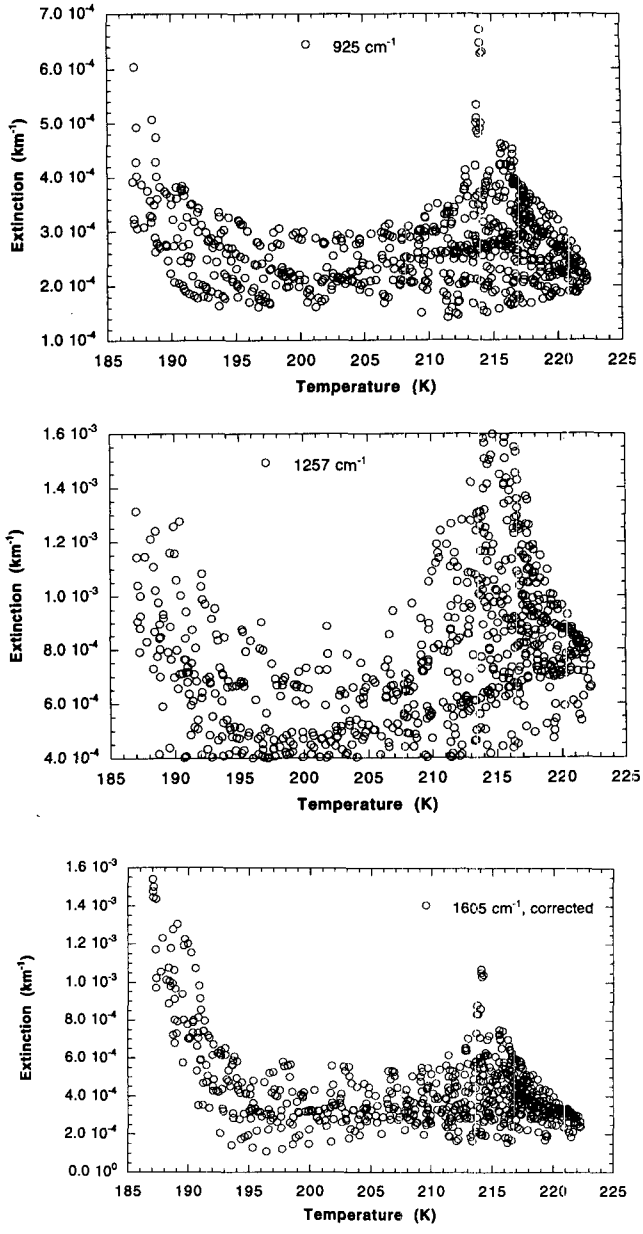

FIG. 13. CLAES daytime extinction (km^{-1}) at 46 hPa (a) at 925 cm^{-1} (10.8 μm), (b) at 1257 cm^{-1} (7.95 μm), and (c) 1605 cm^{-1} (6.23 μm) on 18 August 1992 using all longitudes for latitudes between 76 and 32°S, graphed as a function of temperature. The extinction data at 1605 cm^{-1} were corrected for the pressure-induced continuum of oxygen.

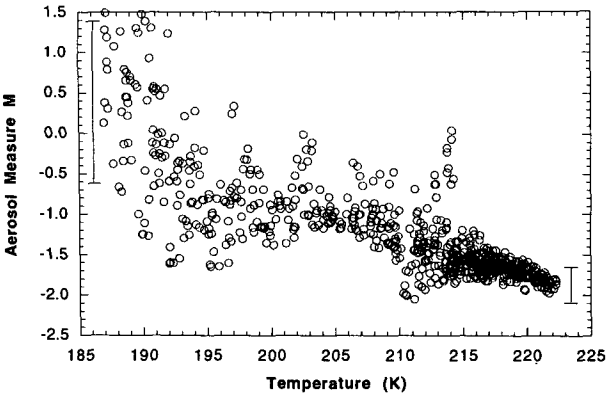

FIG. 14. Aerosol spectral measure M values on 18 August 1992 for the latitude range 76° to 32°S at 46 hPa (near 20 km), graphed as a function of temperature. Theoretical calculations suggest that sulfate and PSC particles have M values less than -1 and greater than 0, respectively. Error bars for the spectral measures of the sulfate and PSC particles are ± 0.2 and ± 1.0, respectively.

TABLE 3. Aerosol measure M values for sulfate/PSC mixtures.

Sulfate portion	M
1.0	−1.75
0.9	−1.47
0.8	−1.19
0.7	−0.91
0.6	−0.62
0.5	−0.33
0.4	−0.04
0.3	+0.26
0.2	+0.55
0.1	+0.85
0.0	+1.15

the aerosol extinction at 1605 cm^{-1} is five times smaller than the 1605 cm^{-1} extinction at 68 and 31 hPa, and so the 21-hPa extinction has larger error bars.

There are some outliers apparent in Fig. 14. For temperatures between 205 and 215 K, there are data points with M values greater than -0.7. These data points in general correspond to aerosol with extinction greater than 6.0×10^{-4} and 7.0×10^{-4} at 925 and 1605 cm^{-1} (see Figs. 13a and 13b). These high values lie outside the majority of the extinction values for the 205–215-K temperature range and are likely retrieval artifacts. The large M values in Fig. 14 for temperatures greater than 205 K are likely spurious.

The sulfate aerosol in Fig. 14 shows a trend in which the aerosol spectral measure M decreases as the temperature decreases. This is a consequence of H_2SO_4 thermodynamics. Steele and Hamill (1981) calculated theoretically that the percent concentration of H_2SO_4 decreases as the temperature decreases and as the water content of the aerosol increases. From Fig. 1 it is apparent that the sulfate spectrum becomes flatter as the H_2SO_4 concentration decreases. In terms of the aerosol spectral measure, M decreases as the H_2SO_4 concentration decreases. For Fig. 14, the H_2O mixing ratio at 46 hPa is near 4.3 ppmv for temperatures greater than 200 K. By the calculations of Steele and Hamill, the H_2SO_4 concentrations are then 60%, 69%, and 75% at temperatures of 200, 210, and 220 K. Based upon the theoretical Mie calculations and the Palmer and Williams (1975) indexes, the M values are -1.3, -1.6, and -1.7 for these three conditions. From Fig. 14, the observed M values are -0.8, -1.3, and -1.8. The two sets of numbers are in qualitative agreement in following the same trend, but diverge in quantitative value as the temperature decreases. As discussed in section 3, there is uncertainty in the indexes of refraction of the sulfate aerosol at low temperatures. If the Palmer and Williams imaginary indexes are increased by 25% at 925 cm^{-1}, and by 5% at 1257 and 1605 cm^{-1}, to more closely agree with the Remsberg et al. (1974) measurements, then the theoretical M values become -1.1, -1.4, and

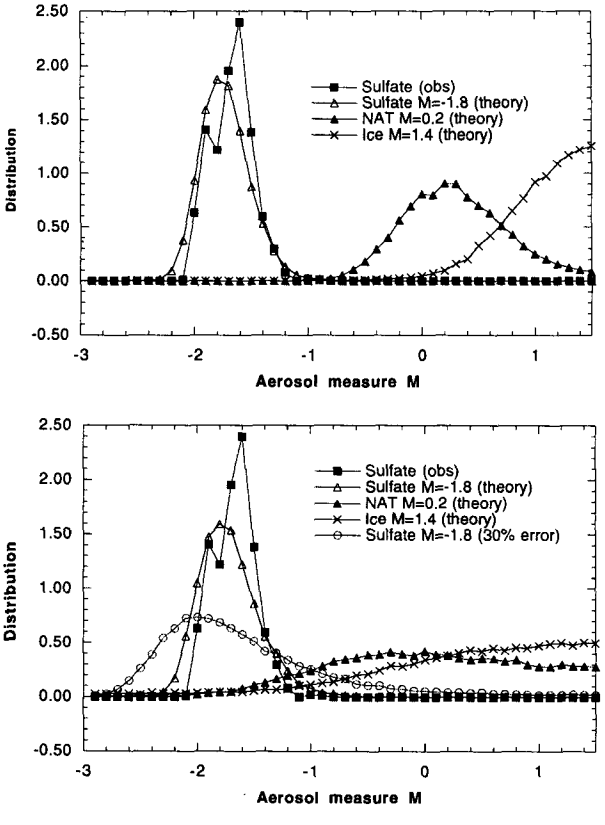

FIG. 15. Distributions of observed and predicted aerosol measure M values. In (a) the theoretical curves are based upon random perturbations of $\pm 10\%$ of the aerosol extinctions. The "Sulfate (obs)" curve is the observed distribution of the data displayed in Fig. 7. In (b) the theoretical curves are based upon random perturbations of the aerosol extinctions, based upon the error bars associated with the 20°N sulfate data and the extinction data between 68° and 72°S. The distributions are normalized by requiring the integrals of the distributions over M to be equal to unity.

-1.5. This adjustment brings theory and observation closer to each other, but there is still disagreement. Resolution of these quantitative details awaits quantification of the sulfuric acid refractive indexes at low temperatures.

The error bars of the aerosol measure M, displayed in Fig. 14, are derived from the distributions of M presented in Fig. 15b. To produce these distributions, aerosol extinctions at 925, 1257, and 1605 cm^{-1} were specified for representative sulfate, ice, and NAT particles. The three extinction sets are based upon the observed ($M = -1.8$) sulfate extinction data in Fig. 6, the observed ($M = 0.2$) NAT extinction data of Fig. 11, and the theoretical ($M = 1.4$) ice extinction values of Fig. 2b (curve e). The theoretical distributions in Figs. 15a and 15b were calculated by randomly perturbing the aerosol extinction values at 925, 1257, and 1605 cm^{-1} in numerous realizations. The distributions in Fig. 15a were calculated using $\pm 10\%$ perturbations, while the distributions in Fig. 15b were calculated using perturbations based upon the aerosol extinction error bars discussed in section 2. The perturbations followed Gaussian statistics, and the distributions were normalized by requiring that the integral of each distribution over M be equal to unity.

The "Sulfate (obs)" curve in Fig. 15a displays the observed distribution of the 20°S to 20°N sulfate aerosol, calculated from the data in Fig. 7. The "Sulfate $M = -1.8$ (theory)" curve displays the theoretical distribution based upon $\pm 10\%$ perturbations, applied to the observations presented in Fig. 6. It is apparent that while the observed distribution is somewhat narrower than the theoretical distribution, the two distributions are roughly comparable. Theoretical curves "NAT $M = 0.2$ (theory)" and "Ice $M = 1.4$ (theory)" were calculated using $\pm 10\%$ perturbations applied to the observed extinction data presented in Fig. 11 and the theoretical data of Fig. 2b (curve e). If the error bars for the observed sulfate and PSC extinction data were $\pm 10\%$, then the distributions of M for the sulfate and PSC particles would display little overlap.

PSC extinction error bars, however, are larger than $\pm 10\%$. In section 2, the aerosol extinction quality indicators were used to estimate the error bars for the aerosol extinction. At 925, 1257, and 1605 cm^{-1}, the aerosol extinction error bars are estimated to be 12%, 13%, and 8% for the 20°S to 20°N sulfate aerosol, and 35%, 31%, and 16% for the PSC particles in the polar vortex. In Fig. 15b, the NAT $M = 0.2$ (theory) and Ice $M = 1.4$ (theory) distributions were calculated using random perturbations of $\pm 35\%$, 31%, and 16% (at 925, 1257, and 1605 cm^{-1}, respectively) while the Sulfate $M = -1.8$ (theory) curve is based upon $\pm 12\%$, 13%, and 8% perturbations. The Sulfate $M = -1.8$ (30% error) curve was calculated using $\pm 35\%$, 31%, and 16% perturbations applied to the observed extinctions (from Fig. 6) at 925, 1257, and 1605 cm^{-1}, respectively. The Sulfate (obs) curve, presented in Figs. 15a and 15b, is the observed distribution for the sulfate aerosol for 20°S to 20°N.

For the sulfate aerosol near the equator, the observed Sulfate (obs) and calculated Sulfate $M = -1.8$ (theory) distributions in Fig. 15b do not show significant contributions for M greater than -1. The Sulfate $M = -1.8$ (30% error) theory distribution, which represents sulfate aerosol inside the polar vortex, is negligible for M greater than 0. This distribution, however, predicts nonnegligible occurrences of values of M less than -2, which is not apparent in Fig. 14, so the distribution may not be meaningful. Adopting a conservative viewpoint, we assume that the distribution is meaningful for M greater than -1. The overlap of the sulfate and PSC distribution curves for M between -1 and 0 then gives rise to ambiguity, since the "$M = 1.4$" and "$M = 0.2$" curves for PSCs have significant contributions for M less than 0. For M between -1 and 0, one therefore cannot say whether a data point, for example, the $M = -0.8$ data point at 190 K in Fig. 14, is due to a sulfate or PSC particle (or a combination of the two).

For M greater than zero, the situation is less ambiguous, since the sulfate distributions do not make important contributions. The $M > 0$ data points in Fig. 14 are therefore likely due to PSC particles (and not sulfate particles).

Based upon the distributions in Fig. 15b, an uncertainty of ± 0.2 is assigned to the sulfate ($M < -1$) data points in Fig. 14 for warm temperatures, and an uncertainty of ± 1.0 is assigned to the PSC ($M > 0$) data points at cold temperatures. These error bars were obtained by calculating the range of M that contained 68% of the total area of the Sulfate $M = -1.8$ (theory) and NAT $M = 0.2$ (theory) distributions. The error bars are positioned in Fig. 14. As the quality of the CLAES data improves in later data versions, the identification process for sulfate and PSC aerosol will become more accurate.

8. Thermodynamic arguments

The theoretical calculations suggest that particles with M greater than 0.0 could be NAT particles. There are data points in the upper left-hand portion of Fig. 14 that meet this criterion. To support this result, it is advisable to check that these data points are consistent with the laboratory studies of the thermodynamics of NAT and water ice. Hanson and Mauersberger (1988) studied laboratory NAT for a range of temperature and partial vapor pressures of H_2O and HNO_3 and also studied the phase equilibria for the water ice–HNO_3 system. By knowing the observed atmospheric water vapor partial pressure, one can calculate the frostpoint temperature from Table 1 of Hanson and Mauersberger (1988). If the observed temperature is below the frost point, then the particles are likely to be of the PSC II type. In a similar manner, vapor pressures of H_2O and

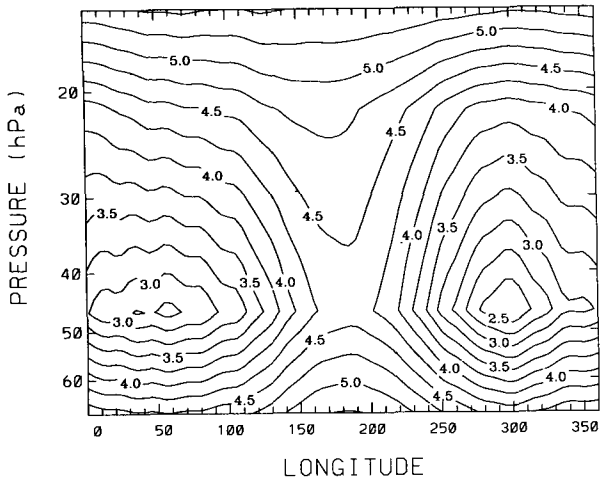

FIG. 16. MLS daytime water vapor mixing ratio values (in ppmv) at 72°S latitude on 18 August 1992 for pressures between 10 and 70 hPa. The MLS H_2O values are influenced by the retrieval climatology at 46 hPa.

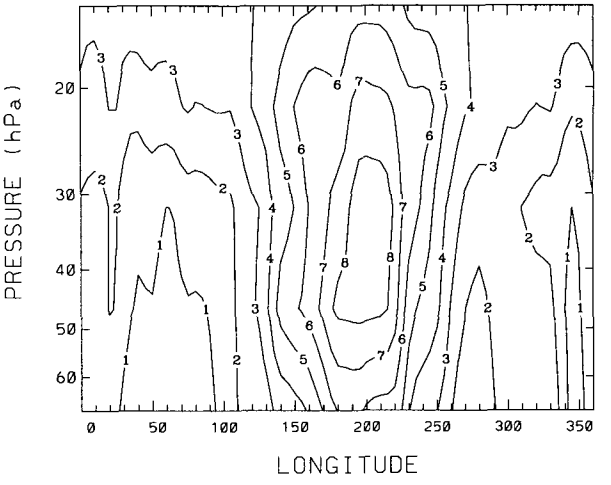

FIG. 17. CLAES daytime HNO_3 mixing ratio values (in ppbv) at 72°S latitude on 18 August 1992 for pressures between 10 and 70 hPa.

HNO_3 predict the expected equilibrium temperature of NAT [see Fig. 1 of Hanson and Mauersberger (1988)]. If the observed temperature is below the NAT equilibrium temperature, and if the observed temperature is above the frostpoint temperature, then the observed particle is likely to be a NAT particle.

To use the Hanson and Mauersberger equations, observed fields of water vapor and nitric acid vapor were mapped using the same sampling and mapping routines as used for the temperature and aerosol fields. Figures 16 and 17 display contour maps of water vapor (from the MLS experiment) and HNO_3 (from the CLAES experiment) for 18 August 1992 at 72°S latitude at 46 hPa. The water vapor amounts are between 3 and 5 ppmv, and the HNO_3 mixing ratios are between 1.4 and 7 ppbv. Low mixing ratio values are observed in the same longitude ranges as for the lowest temperatures displayed in Fig. 9. Lowest mixing ratios are seen near 46 hPa for water vapor and for nitric acid.

The Version 3 MLS water vapor fields are represented as a piecewise linear function with breakpoints at alternate (even numbered) *UARS* pressure surfaces (e.g., at 10, 22, 46 hPa). The water vapor mixing ratios on the odd-numbered surfaces (e.g., 15, 31, 68 hPa) are averages of the mixing ratios on the adjacent even-numbered surfaces. At high latitudes, the estimated uncertainty can increase to 1.8 ppmv at 46 hPa and to 1 ppmv at 22 hPa. Comparisons with other *UARS* data and/or correlative data suggest that MLS H_2O may be 10% to 30% too high in the range 46 to 0.2 hPa (NASA 1994). In Fig. 16, the 46-hPa H_2O data have a quality indicator typically near -1.3 ppmv, signifying that the uncertainty is ± 1.3 ppmv and that the climatological input to the retrieval influences the retrieval by greater than 50%. In a recent study (G. Morris 1993, personal communication), it was found for the polar latitudes that the MLS water vapor mixing ratios were 0.5 ppmv higher than the HALOE retrievals.

While Figs. 9, 10, 16, and 17 refer only to 72°S, these figures are representative for other latitudes and pressure levels inside the polar vortex, for example, latitudes poleward of 63°S. A cold temperature minimum with temperatures below 195 K is located between 20 and 30 hPa, and between 250° and 360° longitude. A smaller temperature minimum is also observed between 20 and 30 hPa for longitudes between 0° and 50°. The H_2O minimum is observed at pressures between 40 and 50 hPa, for longitudes between 250°–360° and 0°–100°. The HNO_3 composition field is characterized by

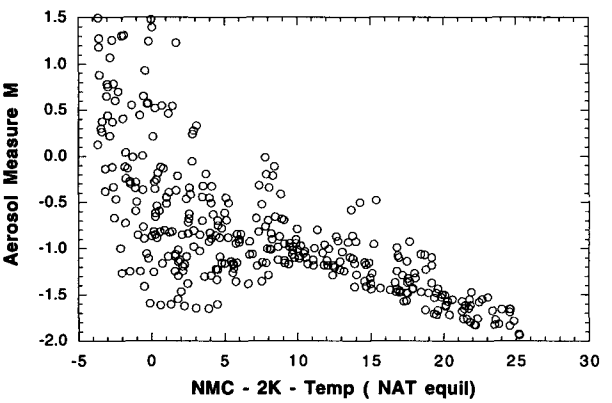

FIG. 18. Temperature differences between the ambient gas temperature and the NAT equilibrium temperature versus aerosol measure M values on 18 August 1992 at 46 hPa and latitudes between 76° and 56°S. The ambient gas temperature is the NMC temperature minus 2 K. Values for H_2O are from the MLS dataset (which is influenced by climatology at 46 hPa). The HNO_3 values are from the CLAES experiment.

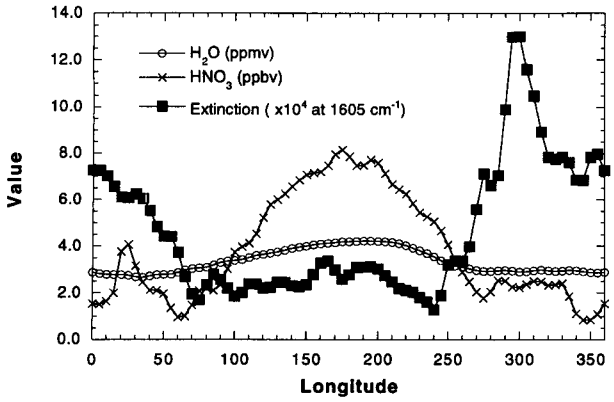

FIG. 19. The longitudinal distribution of H_2O, CLAES HNO_3, and CLAES aerosol 1605 cm^{-1} (6.23 μm) extinction at 46 hPa on 18 August 1992 at 72°S. The MLS H_2O values are influenced by the retrieval climatology at 46 hPa. The 1605 cm^{-1} extinction is corrected for the presence of the pressure-induced absorption of oxygen.

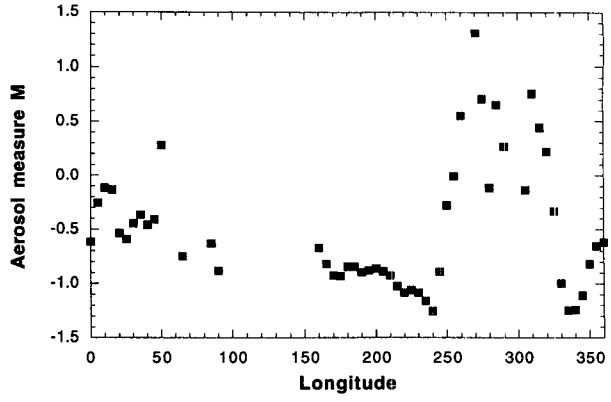

FIG. 20. The longitudinal distribution of aerosol measure M values at 46 hPa on 18 August 1992 at 72°S.

low regions of HNO_3 mixing ratio for pressures greater than 30 hPa and for longitudes between 250°–360° and 0°–100°. Enhanced aerosol extinction is observed for longitudes between 280° and 350° for the 925, 1257, and 1605 cm^{-1} data. The 1605 cm^{-1} extinction is somewhat enhanced between 20 and 100° longitude.

Using the CLAES and MLS data, for latitudes between 76°S and 56°S, Fig. 18 presents CLAES aerosol measure M values for 18 August 1992 at 46 hPa. On the abscissa are values of the temperature difference between the ambient gas temperature and that of the NAT equilibrium temperature. The NAT equilibrium temperature was calculated using the CLAES HNO_3 and MLS H_2O mixing ratios and the formula cited by Hanson and Mauersberger. Two degrees were subtracted from the NMC temperatures since our validation studies, in which radiosonde temperature profiles are compared to U.K. Meteorological Office (UKMO) and to NMC temperature profiles, indicate that UKMO temperatures for the polar latitudes are approximately 2 K lower than the NMC temperatures at 46 hPa and are closer to the radiosonde values. The scatter diagram shows that for temperature differences less than zero that PSC particles (with spectral measure greater than zero) are below the NAT equilibrium temperature. One sees very few air parcels with spectral measure greater than zero and temperatures above the NAT equilibrium temperature. The scatter diagram also shows for particles 10 K above the NAT equilibrium that the spectral measure is mainly less than −1.0 (i.e., that the aerosol particles are sulfate particles).

An examination of the longitudinal structure of the field values of extinction, spectral measure M, H_2O, HNO_3, and the temperature thresholds for NAT and ice particles is presented in Figs. 19–21 at 46 hPa and 72°S. In Fig. 19, values of 1605 cm^{-1} aerosol extinction, CLAES HNO_3, and MLS H_2O mixing ratios are presented. The H_2O values change slightly along the latitude circle. The aerosol extinction at 1605 cm^{-1} peaks near 300° longitude. In contrast, a decrease is observed in the HNO_3 values for longitudes greater than 200°. To first approximation, parcels at 72°S rotate clockwise around the South Pole. Global atmospheric circulation statistics (Randel 1992) specify a zonal wind speed of the order of 40–50 m s^{-1} at 50 hPa at latitudes over the Palmer Peninsula for the July–October time frame. This flow speed implies that a parcel takes roughly one day to travel between 240° and 360° longitude, and that this timescale sets temporal limits for the PSC formation process. As air parcels travel along the latitude circle, they become depleted in gas phase HNO_3 as PSC particles are formed from the H_2O and HNO_3 gas phase. (For the 460-K potential temperature surface, a parcel moves along the 72°S latitude circle, experiencing a change in pressure between 38 and 54 hPa. Figure 19 approximately traces the changes

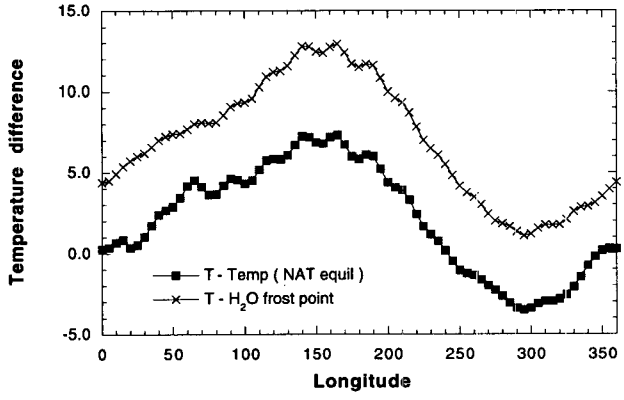

FIG. 21. The longitudinal distribution of temperature differences for the water frostpoint and NAT equilibrium at 46 hPa on 18 August 1992 at 72°S. Air parcels are at a temperature above the water frostpoint at all longitudes, and below the NAT equilibrium temperature between 240° and 340° longitude.

in H_2O and HNO_3 experienced by a parcel as it moves along a latitude circle in the Antarctic vortex.) Spectral measure M values for the CLAES aerosol are presented in Fig. 20 along the 72°S latitude circle. Positive M values mark the location of PSC particles, for the longitude range 250°–330°. This pattern is of course related to the histogram presented in Fig. 12b for a wider range of polar latitudes.

Assuming axisymmetric flow around the South Pole, Fig. 19 suggests that 6 ppbv of HNO_3 goes from the gas phase into the aerosol phase (or is transformed into other gas phase species) as a parcel moves from 150° to 300° longitude. At the same time, the aerosol extinction increases by 1×10^{-3} km^{-1} at 1605 cm^{-1}. As a check upon the plausibility of this transformation, it is necessary to relate the 6 ppbv gas phase value with the amount of HNO_3 tied up in the aerosol, assuming that the aerosol is composed of NAT. To do this, the two dozen NAT size distributions of Hofmann and Deshler (1991) and Deshler et al. (1991) were used to graph 1605 cm^{-1} extinction values (based upon Mie calculations) versus equivalent HNO_3 mixing ratios. An equivalent HNO_3 mixing ratio, f_{HNO_3}, was calculated from the bimodal size distribution, the NAT mass density, and the ambient temperature and pressure for each of the in situ observations. The size distributions yielded a range of extinction (from 9×10^{-6} to 1.2×10^{-3} km^{-1}) and a range of equivalent HNO_3 mixing ratio for the aerosol (between f_{HNO_3} of 0.25 and 9.8 ppbv). To obtain the average equivalent HNO_3 mixing ratio, extinctions with values greater than 2.0×10^{-4} km^{-1} (matching the lower bounds displayed in Fig. 13) were scaled to 1.0×10^{-3} km^{-1}. Scaling the extinction values to 1.0×10^{-3} km^{-1}, and the f_{HNO_3} values by the same scaling factors, the NAT size distributions produced equivalent HNO_3 mixing ratios between 1 and 14 ppbv, with an average near 6 ppbv. Therefore, it is plausible that the decrease in the gas phase HNO_3 and the increase in aerosol extinction displayed in Fig. 19 do represent the conversion of HNO_3 into NAT.

Thermodynamic threshold calculations can also help to identify the composition of the PSC particles in Fig. 20. Figure 21 displays temperature differences for the water frostpoint and NAT equilibrium thresholds. The curves specify the difference in the ambient gas temperature and the threshold temperatures for the ice frostpoint and that for NAT. The calculations were carried out in the same way as in Fig. 18; the NMC temperatures have been reduced by 2 K. It is apparent that the parcels in Fig. 21 are above the ice frostpoint for all longitudes. Parcels for the 240°–350° longitude range are below the NAT equilibrium threshold. As discussed above, the H_2O mixing ratios used in the calculation are likely to be high by 0.5 ppmv. A calculation with H_2O mixing ratios reduced by 0.5 ppmv would produce lower frostpoint temperatures (which would lead to more positive temperature differences in Fig. 21, for the ice frostpoint). Therefore, the enhanced extinction in Fig. 19 and the positive spectral M values in Fig. 20 most likely indicate the location of NAT particles.

9. Summary

The sections above illustrate a technique that uses multiwavelength aerosol extinction observations to locate sulfate and PSC particles. Observations at only three wavenumbers are used in this paper. The use of CLAES extinction data at several additional wavenumbers, as well as the use of more extensive techniques, is possible. Yet, with observations at three wavenumbers, it is possible to form an aerosol measure M that is independent of the magnitude of the aerosol extinction and differs for the sulfate and PSC particles. Figures presented above demonstrate that the spectral shape of the atmospheric aerosol, quantified by the aerosol measure M, changes between middle and high latitudes, that these changes are consistent with theoretical aerosol spectra for sulfate and PSC particles and that the M values associated with the particles in the polar latitudes have associated temperature, gas phase H_2O and HNO_3 mixing ratios consistent with laboratory thermodynamic equilibrium studies of NAT. This technique opens up the possibility of monitoring from orbit using infrared sensors the location, onset, and occurrence rate of PSCs, which play an important role in the development and evolution of the Antarctic ozone hole.

Acknowledgments. Research at NCAR was supported by the NASA *UARS* program under Contract S-10782-C. NCAR is sponsored by the National Science Foundation. Work at the Lockheed Palo Alto Research Laboratory was supported by NASA under Contract NAS5-27752. The MLS experiment was supported by NASA, the U.K. Science and Engineering Research Council, and the British National Space Center, for work performed at the Jet Propulsion Laboratory, at the Rutherford Appleton Laboratory, Heriot-Watt University, and at Edinburgh University, respectively. Appreciation is expressed to T. Deshler (University of Wyoming) who has provided aerosol size distributions to the *UARS* research groups. Acknowledgment is extended to the reviewer who suggested the error analysis presented in Figs. 15a and 15b.

REFERENCES

Ackerman, S. A., W. L. Smith, J. D. Spinhirne, and H. E. Revercomb, 1990: The 27–28 October 1986 FIRE IFO cirrus case study: Spectral properties of cirrus clouds in the 8–12 μm window. *Mon. Wea. Rev.*, **118,** 2377–2388.

Barber, P. W., and S. C. Hill, 1990: *Light Scattering by Particles. Computational Methods.* World Scientific, 261 pp.

Browell, E. V., C. F. Butler, S. Ismail, P. A. Robinette, A. F. Carter, N. S. Higdon, O. B. Toon, M. R. Schoeberl, and A. F. Tuck, 1990: Airborne lidar observations in the wintertime Arctic stratosphere: Polar stratospheric clouds. *Geophys. Res. Lett.*, **17,** 385–388.

Cressman, G. P., 1959: An operational objective analysis system. *Mon. Wea. Rev.*, **87,** 367–374.

Crutzen, P. J., and F. Arnold, 1986: Nitric acid cloud formation in the cold Antarctic stratosphere: A major cause for the springtime 'ozone hole.' *Nature,* **324,** 651–655.

Deshler, T., A. Adrian, D. J. Hofmann, and G. P. Gobbi, 1991: Evidence for denitrification in the 1990 Antarctic spring stratosphere: II. Lidar and aerosol measurements. *Geophys. Res. Lett.,* **18,** 1999–2002.

——, B. J. Johnson, and W. R. Rozier, 1993: Balloonborne measurements of Pinatubo aerosol during 1991 and 1992 at 41°N: Vertical profiles, size distributions, and volatility. *Geophys. Res. Lett.,* **20,** 1435–1438.

Feynman, R. P., 1964: Refractive index of dense materials. *The Feynman Lectures on Physics.* Vol. II. Addison-Wesley, 32-1–32-13.

Goodman, J., O. B. Toon, R. F. Pueschel, K. G. Snetsinger, and S. Verma, 1989: Antarctic stratospheric ice crystals. *J. Geophys. Res.,* **94,** 16 449–16 457.

Grainger, R. G., A. Lambert, F. W. Taylor, J. J. Remedios, C. D. Rodgers, and M. Corney, 1993: Infrared absorption of volcanic stratospheric aerosols observed by ISAMS. *Geophys. Res. Lett.,* **20,** 1283–1286.

Halperin, B., and D. G. Murcray, 1987: Effect of volcanic aerosols on stratospheric radiance at wavelengths between 8 and 13 μm. *Appl. Opt.,* **26,** 2222–2235.

Hanson, D., and K. Mauersberger, 1988: Laboratory studies of the nitric acid trihydrate: Implications for the polar stratosphere. *Geophys. Res. Lett.,* **15,** 855–858.

Hervig, M. E., J. M. Russell III, L. L. Gordley, J. H. Park, and S. R. Drayson, 1993: Observations of aerosol by the HALOE experiment onboard UARS: A preliminary validation. *Geophys. Res. Lett.,* **20,** 1291–1294.

Hofmann, D. J., and T. Deshler, 1991: Stratospheric cloud observations during formation of the Antarctic ozone hole in 1989. *J. Geophys. Res.,* **96,** 2897–2912.

Kalman, R. E., 1960: A new approach to linear filtering and prediction problems. *J. Basic Eng.,* **820,** 35–45.

Kinne, S., O. B. Toon, G. C. Toon, C. B. Farmer, E. V. Browell, and M. P. McCormick, 1989: Measurements of size and composition of particles in polar stratospheric clouds from infrared solar absorption spectra. *J. Geophys. Res.,* **94,** 16 481–16 491.

Lambert, A., R. G. Grainger, J. J. Remedios, C. D. Rodgers, M. Corney, and F. W. Taylor, 1993: Measurements of the evolution of the Mt. Pinatubo aerosol cloud by ISAMS. *Geophys. Res. Lett.,* **20,** 1287–1290.

McCormick, M. P., and C. R. Trepte, 1986: SAM II measurements of Antarctic PSCs and aerosols. *Geophys. Res. Lett.,* **13,** 1276–1279.

——, H. M. Steele, P. Hamill, W. P. Chu, and T. J. Swissler, 1982: Polar stratospheric cloud sightings by SAM II. *J. Atmos. Sci.,* **39,** 1387–1397.

——, C. R. Trepte, and M. C. Pitts, 1989: Persistence of polar stratospheric clouds in the southern polar region. *J. Geophys. Res.,* **94,** 11 241–11 251.

Mergenthaler, J. L., J. B. Kumer, and A. E. Roche, 1993: CLAES south-looking aerosol observations for 1992. *Geophys. Res. Lett.,* **20,** 1295–1298.

Middlebrook, A. M., L. T. Iraci, L. S. McNeil, B. G. Koehler, M. A. Wislon, O. W. Saastad, and M. A. Tolbert, 1993: Fourier transform–infrared studies of thin H_2SO_4/H_2O films: Formation, water uptake, and solid–liquid phase changes. *J. Geophys. Res.,* **98,** 20 473–20 481.

Molina, M. J., R. Zhang, P. J. Wooldridge, J. R. McMahon, J. E. Kim, H. Y. Chang, and K. D. Beyer, 1993: Physical chemistry of the $H_2SO_4/HNO_3/H_2O$ system: Implications for polar stratospheric clouds. *Science,* **261,** 1418–1423.

NASA, 1994: Upper Atmosphere Research Satellite validation report, in preparation.

Orlando, J. J., G. S. Tyndall, K. E. Nickerson, and J. G. Calvert, 1991: The temperature dependence of collision-induced absorption by oxygen near 6 μm. *J. Geophys. Res.,* **96,** 20 755–20 760.

Palmer, K. F., and D. Williams, 1975: Optical constants of sulfuric acid; application to the clouds of Venus? *Appl. Opt.,* **14,** 208–219.

Pinkley, L. W., and D. Williams, 1976: The infrared optical constants of sulfuric acid at 250 K. *J. Opt. Soc. Amer.,* **66,** 122–124.

Pollack, J. B., F. C. Witteborn, K. O'Brien, and B. Flynn, 1991: A determination of the infrared optical depth of the El Chichón volcanic cloud. *J. Geophys. Res.,* **96,** 3115–3122.

Pueschel, R. F., G. V. Ferry, K. G. Snetsinger, J. Goodman, J. E. Dye, D. Baumgardner, and B. W. Gandrud, 1992: A case of type I polar stratospheric cloud formation by heterogeneous nucleation. *J. Geophys. Res.,* **97,** 8105–8114.

Randel, W. J., 1992: Global atmospheric circulation statistics, 1000–1 mb. NCAR Tech. Note NCAR/TN-366+STR, 256 pp.

Read, W. G., L. Froidevaux, and J. W. Waters, 1993: Microwave limb sounder measurements of stratospheric SO_2 from the Mt. Pinatubo volcano. *Geophys. Res. Lett.,* **20,** 1299–1302.

Reber, C. A., C. E. Trevathan, R. J. McNeal, and M. R. Luther, 1993: The Upper Atmosphere Research Satellite (UARS) Mission. *J. Geophys. Res.,* **98,** 10 643–10 647.

Remsberg, E. E., D. Lavery, and B. Crawford, 1974: Optical constants for sulfuric and nitric acids. *J. Chem. Eng. Data,* **19,** 263–266.

Roche, A. E., J. B. Kumer, J. L. Mergenthaler, G. A. Ely, W. G. Uplinger, J. F. Potter, T. C. James, and L. W. Sterritt, 1993: The cryogenic limb array etalon spectrometer (CLAES) on UARS: Experiment description and performance. *J. Geophys. Res.,* **98,** 10 763–10 775.

Smith, W. L., X. L. Ma, S. A. Ackerman, H. E. Revercomb, and R. O. Knuteson, 1993: Remote sensing cloud properties from high spectral resolution infrared observations. *J. Atmos. Sci.,* **50,** 1708–1720.

Solomon, S., R. Garcia, F. S. Rowland, and D. Wuebbles, 1986: On the depletion of Antarctic ozone. *Nature,* **321,** 755–758.

Steele, H. M., and P. Hamill, 1981: Effects of temperature and humidity on the growth and optical properties of sulphuric acid–water droplets in the stratosphere. *J. Aerosol. Sci.,* **12,** 517–528.

Taesler, I., 1975: Hydrogen bond studies, XCIV: Diaquaoxonium ion in nitric acid tryhydrate. *Acta Crystallogr. Sect. B,* **31,** 1489–1495.

Tolbert, M. A., and A. M. Middlebrook, 1990: Fourier transform infrared studies of model polar stratospheric cloud surfaces: Growth and evaporation of ice and nitric acid/ice. *J. Geophys. Res.,* **95,** 22 423–22 431.

Toon, O. B., P. Hamill, R. P. Turco, and J. Pinto, 1986: Condensation of HNO_3 and HCl in the winter polar stratosphere. *Geophys. Res. Lett.,* **13,** 1284–1287.

——, E. V. Browell, S. Kinne, and J. Jordan, 1990: An analysis of lidar observations of polar stratospheric clouds. *Geophys. Res. Lett.,* **17,** 393–396.

Turco, R. P., O. B. Toon, and P. Hamill, 1989: Heterogeneous physicochemistry of the polar ozone hole. *J. Geophys. Res.,* **94,** 16 493–16 510.

van de Hulst, H. C., 1975: *Light Scattering by Small Particles.* Wiley, 470 pp.

Warren, S. G., 1984: Optical constants of ice from the ultraviolet to the microwave. *Appl. Opt.,* **23,** 1206–1225.

Waters, J. W., L. Froidevaux, W. G. Read, G. L. Manney, L. S. Elson, D. A. Flower, R. F. Jarnot, and R. S. Harwood, 1993: Stratospheric ClO and ozone from the Microwave Limb Sounder on the Upper Atmosphere Research Satellite. *Nature,* **362,** 597–602.

Watterson, I. G., and A. F. Tuck, 1989: A comparison of the longitudinal distributions of polar stratospheric clouds and temperatures for the 1987 Antarctic spring. *J. Geophys. Res.,* **94,** 16 511–16 525.

WMO, 1991: Scientific assessment of ozone depletion: 1991. World Meteorological Organization.